Journal of the Mechanics and Physics of Solids 61 (2013) 1737–1752

Contents lists available at SciVerse ScienceDirect

Journal of the Mechanics and Physics of Solids

journal homepage: www.elsevier.com/locate/jmps

Experiments and viscoelastic analysis of peel test with patterned strips for applications to transfer printing

Hang Chen [a,b], Xue Feng [a,b,*], Yin Huang [a,b], Yonggang Huang [c,d,**], John A. Rogers [e]

[a] AML, Department of Engineering Mechanics, Tsinghua University, Beijing 100084, China
[b] Center for Mechanics and Materials, Tsinghua University, Beijing 100084, China
[c] Department of Civil and Environmental Engineering, Northwestern University, Evanston, IL 60822, USA
[d] Department of Mechanical Engineering, Northwestern University, Evanston, IL 60822, USA
[e] Department of Materials Science and Engineering, University of Illinois, Urbana, IL 60208, USA

ARTICLE INFO

Article history:
Received 5 January 2013
Received in revised form
20 March 2013
Accepted 3 April 2013
Available online 15 April 2013

Keywords:
Viscoelasticity
Peel test
Patterned strips
Energy release rate

ABSTRACT

Transfer printing is an exceptionally sophisticated approach to assembly and micro-/nanofabrication that relies on a soft, elastomeric 'stamp' to transfer solid, micro-/nanoscale materials or device components from one substrate to another, in a large-scale, parallel fashion. The most critical control parameter in transfer printing is the strength of adhesion between the stamp and materials/devices. Conventional peel tests provide effective and robust means for determining the interfacial adhesion strength, or equivalently the energy release rate, and its dependence on peel speed. The results presented here provide analytic solutions for tests of this type, performed using viscoelastic strips with and without patterns of relief on their surfaces, and validated by systematic experiments. For a flat strip, a simple method enables determination of the energy release rate as a function of the peel speed. Patterned strips can be designed to achieve desired interfacial properties, with either stronger or weaker adhesion than that for a flat strip. The pattern spacing influences the energy release rate, to give values that initially decrease to levels smaller than those for a corresponding flat strip, as the pattern spacing increases. Once the spacing reaches a critical value, the relief self-collapses onto the substrate, thereby significantly increasing the contact area and the strength of adhesion. Analytic solutions capture not only these behaviors, as confirmed by experiment, but also extend to strips with nearly any pattern geometry of cylindrical pillars.

1. Introduction

Transfer printing is an exceptionally sophisticated approach to assembly and micro-/nanofabrication that relies on a soft, elastomeric 'stamp' to retrieve solid, micro/nanoscale materials or device components from one substrate to print on a target substrate, in a large-scale, parallel fashion (Carlson et al., 2012a). This scheme creates a wide range of application opportunities through its ability to separate requirements associated with source and receiver substrates, and to enable heterogeneous integration of dissimilar materials into well-controlled two and three dimensional architectures. Enabled

* Corresponding author at: AML, Department of Engineering Mechanics, Tsinghua University, Beijing 100084, China.
** Corresponding author at: Department of Civil and Environmental Engineering, Northwestern University, Evanston, IL 60822, USA.
E-mail addresses: fengxue@tsinghua.edu.cn (X. Feng), y-huang@northwestern.edu (Y. Huang).

0022-5096/$ - see front matter © 2013 Elsevier Ltd. All rights reserved.
http://dx.doi.org/10.1016/j.jmps.2013.04.001

devices range from cameras that use biologically inspired designs to achieve superior performance (Ko et al., 2008; Jung et al., 2010), to surgical and diagnostic tools that naturally integrate with the human body to provide advanced therapeutic capabilities (Someya et al., 2004; Kim et al., 2010a, 2010b, 2011a, 2011b; Viventi et al., 2010, 2011). The key challenge in efficient operation of transfer printing is to enable mechanisms for switching the strength of adhesion to the surface of the stamp, from strong to weak to facilitate the first and second steps of the process. Several strategies have been developed:

1) *kinetically-controlled transfer printing* (Meitl et al., 2006; Feng et al., 2007): here, the stamp is retracted rapidly during the first step, and slowly during the second, to make use of the strong and weak adhesion that occurs in these two regimes due to viscoelasticity of the materials used for the stamps;
2) *surface-relief-assisted transfer printing* (Kim et al., 2010c; Wu et al., 2011; Kim et al., 2012; Yang et al., 2012): here, strategically design structures of surface relief, such as sharp, pyramidal microtips at appropriate spacings, enable large and small contact areas during the first and second steps, respectively, as a means to control adhesion;
3) *shear-enhanced transfer printing* (Carlson et al., 2011; Cheng et al., 2012): here, degree of shear loading controls initiation of cracks at the edges of contact areas; low and high loadings yield strong and weak adhesion, respectively;
4) *laser-driven transfer printing* (Li et al., 2012a, 2012b; Saeidpourazar et al., 2012): here, a laser pulse creates local heating at the interface, to initiate separation by forces that arise from the large mismatch in coefficients of thermal expansion in the stamp and adhered materials/devices; and
5) *pneumatic-driven transfer printing* (Carlson et al., 2012b): here, the adhesion is modulated by pressurizing microchannels near the surface of the stamp, to affect release.

In all schemes, the mechanics and materials science associated with interfacial adhesion are critically important. Generally, the adhesion force is a constant (not "tunable") for an interface between two elastic materials, but may depend on the speed of interfacial delamination if one (or both) of the constituent(s) is (are) viscoelastic (Gent and Schultz, 1972; Maugis and Barquins, 1978; Tsai and Kim, 1993; Barquins and Ciccotti, 1997; Barthel and Roux, 2000). Surface textures that mimic gecko foot-hairs, can substantially increase the adhesion. Gao and Yao (2004) and Yao and Gao (2006) identified the basis mechanism of robust and releasable adhesion in biology. Geim et al. (2003) demonstrated that arrays of circular pillars can yield non-specific adhesion capable of supporting large weights. Substantial increase of adhesion has also been observed in the indentation experiments of arrays of circular pillars (Crosby et al., 2005), and in the peel tests of arrays of circular (Lamblet et al., 2007; Poulard et al., 2011), square and triangular pillars (Lamblet et al., 2007). Such approaches have been successfully applied in transfer printing (Kim et al., 2010c; Kim et al., 2012; Yang et al., 2012). Quantitative study of these and related effects by Arzt et al. (2003) in the context of gecko foot-hairs and by Persson and Gorb (2003) and Hui et al. (2005) in the context of patterned strips used the JKR model (Johnson et al., 1971). Such models, however, all assume linear elastic behavior in the materials. Such assumptions may not be valid for viscoelastic materials such as polydimethylsiloxane (PDMS) which is widely used in transfer printing; in fact, viscoelasticity is critically important for the kinetically-controlled and surface-relief-assisted schemes outlined above.

The peel test provides an effective and robust method to determine the adhesion strength of an interface between an elastic strip and an elastic substrate (Kendall, 1975; Brown, 1991; Gent, 1996). As illustrated in Fig. 1, a peel force (at a given peel angle) delaminates the strip from the underlying substrate. For steady-state peeling, the interfacial adhesion strength is obtained analytically from the measured peel force based on energy balance (Spies, 1953; Bikerman, 1957; Kaeble, 1959, 1960; Jouwersma, 1960; Yurenka, 1962; Gardon, 1963; Kendall, 1973; Nicholson, 1977). Such an approach has been extended to an elastic–plastic strip (e.g., Kim and Aravas, 1988; Kim et al., 1989), but is not readily applicable to peeling of a viscoelastic strip.

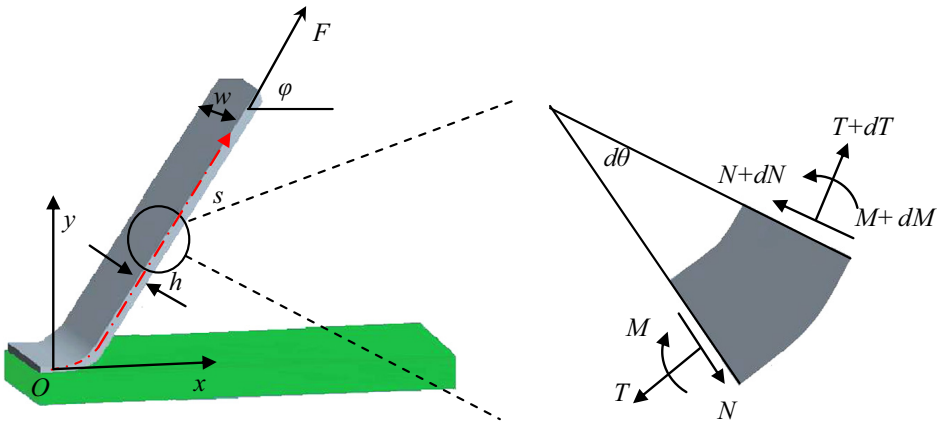

Fig. 1. Schematic illustration of an elastomeric strip in the peel test.

This paper aims at determining the interfacial adhesion for a viscoelastic strip on a rigid substrate, and establishing schemes for tuning the interfacial adhesion via patterned strips, both in the context of applications in transfer printing. A theory for the peel test is established in Section 2 for a flat, viscoelastic strip. The theory is extended to patterned strips in Section 3 to study its effect on the interfacial adhesion (e.g., pillar height, size, spacing and distribution). The analytic model is validated by experiments in Section 4. It is shown that one can design patterned strips to achieve the desired interfacial adhesion, which can be stronger, or weaker, than the adhesion for a flat strip (without patterns). Different patterns (shape and spacing) are discussed in Section 5.

2. Interfacial adhesion of a linear viscoelastic strip

Fig. 1 shows a schematic illustration of the peel test for a linear viscoelastic strip bonded to a stiff substrate. The strip is subjected to a peel force F at a peel angle ϕ. Peeling of the strip is modeled by the delamination of strip/substrate interface, and the strip is modeled as a beam of thickness h and width w (Fig. 1). Let (x,y) denote the local coordinate with the origin at the tip (front) of the interfacial crack (Fig. 1). Any point on the strip can also be represented by the arc length S and tangential angle θ, which are related to (x,y) by $ds=\sqrt{(dx)^2+(dy)^2}$ and $\tan\theta=dy/dx$. For steady-state peeling, the strip has a constant shape such that $\theta=\theta(s)$ does not change with time, and the tangent at the end of strip is parallel to the peel force F.

2.1. Equilibrium equations

Equilibrium of forces in the strip gives the axial force $T=F\cos(\phi-\theta)$ and shear force $N=F\sin(\phi-\theta)$ (Fig. 1). Let M denote the bending moment, which does not change with time, $M=M(s)$, for steady-state peeling. Equilibrium of bending moments in the strip requires $dM/ds+N=0$, which gives (Kim and Aravas, 1988)

$$\frac{dM}{ds}+F\sin[\phi-\theta(s)]=0, \tag{1}$$

the boundary condition at the tip of the strip is

$$\theta(s=0)=0, \tag{2}$$

because the rigid substrate does not deform. The boundary condition at the other end where the peel force is applied, under the steady-state condition, is

$$\theta(s\to\infty)=\phi. \tag{3}$$

2.2. Viscoelastic model

The axial and shear forces, bending moment, curvature $\kappa=d\theta/ds$, and membrane strain ε_m in the strip all depend only on the arc length s at the steady-state. Their rates of change (e.g., $\dot{\kappa}$) can be related to the derivative with respect to s (Loukis and Aravas, 1991), i.e.,

$$\dot{\kappa}dt=\frac{d\kappa}{ds}ds. \tag{4}$$

The bending moment is related to the curvature k in the strip by (Christensen, 2003)

$$M=I\int_0^t E(t-\tau)\frac{d\kappa}{d\tau}d\tau, \tag{5}$$

where $I=wh^3/12$ is the moment of inertia of the cross section, and the relaxation modulus $E(t)$ depends on time. It has a representative form

$$E(t)=E(\infty)+[E(0)-E(\infty)]\exp\left(-\frac{t}{t_c}\right), \tag{6}$$

where $E(0)$ and $E(\infty)$ are the initial relaxation and long-time asymptote moduli, respectively, and t_c is the relaxation time.

For steady-state peeling, the tangential velocity of the strip is given by (Tsai and Kim, 1993; also see details in Appendix A)

$$v(s)=\frac{1+\varepsilon_m(s)}{1+\varepsilon_{peel}}v_{peel}, \tag{7}$$

where ε_{peel} and v_{peel} are the membrane strain and speed at the end of the strip, respectively. The crack tip speed is $v_{crack}=v(0)=v_{peel}[1+\varepsilon_m(0)]/(1+\varepsilon_{peel})$ such that Eq. (7) becomes $v(s)=v_{crack}[1+\varepsilon_m(s)]/[1+\varepsilon_m(0)]$, which is approximately constant $v(s)\approx v_{crack}$ since the membrane strain ε_m is usually much less than 1. Time t then corresponds to the arc length

$s = v_{crack}t$, and Eq. (5) then becomes

$$M(s) = I\int_0^s E\left(\frac{s-l}{v_{crack}}\right)\frac{d\kappa}{dl}dl = I\left[E(0)\kappa(s) + \frac{1}{v_{crack}}\int_0^s \kappa(l)E'\left(\frac{s-l}{v_{crack}}\right)dl\right]. \tag{8}$$

Substitution of Eq. (8) into Eq. (1) gives

$$v_{crack}E(0)\frac{d^2\theta}{ds^2} + E'\left(\frac{s}{v_{crack}}\right)\frac{d\theta}{ds}\bigg|_{s=0} + \int_0^s E'\left(\frac{s-l}{v_{crack}}\right)\frac{d^2\theta}{dl^2}dl + v_{crack}\frac{F}{I}\sin(\phi-\theta) = 0, \tag{9}$$

where $E'(t) = dE/dt$. This is a second-order differential–integral equation, with the boundary conditions in Eqs. (2) and (3). It is solved numerically by the shooting method, i.e., assume a value of $(d\theta/ds)_{s=0}$, solve Eq. (9) with the condition $\theta_{s=0} = 0$ in Eq. (2), to satisfy the other condition $\theta_{s\to\infty} = \phi$ in Eq. (3). Dimensional analysis of Eq. (9) shows that θ depends on the normalized arc length and peel force, and takes the form

$$\theta = \theta\left[\frac{s}{v_{crack}t_c}, \frac{(v_{crack}t_c)^2F}{E(0)I}, \phi, \frac{E(\infty)}{E(0)}\right], \tag{10}$$

where $v_{crack}t_c$ is the length of interfacial delamination over the relaxation time in viscoelasticity. Fig. 2 shows θ versus the normalized arc length for vertical peeling ($\phi = 90^\circ$), and normalized peel force ranging from 0.046 to 4.4. The ratio of initial relaxation to long-time asymptote moduli is $E(\infty)/E(0) = 0.92$ for PDMS mixed at 10:1 ratio (Lin et al., 2008). The tangential angle θ reaches the peel angle (90°) when the arc length is approximately $50v_{crack}t_c$, and it increases rapidly with the peel force. Fig. 3 shows the profile of the strip, normalized by $v_{crack}t_c$, for several normalized peel forces.

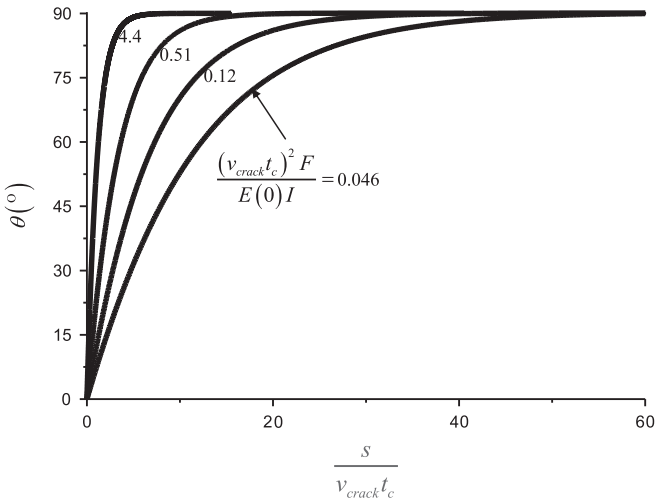

Fig. 2. The angle θ versus normalized arc length for vertical peeling ($\phi = 90^\circ$) and $E(\infty)/E(0) = 0.92$ at several normalized peeling forces.

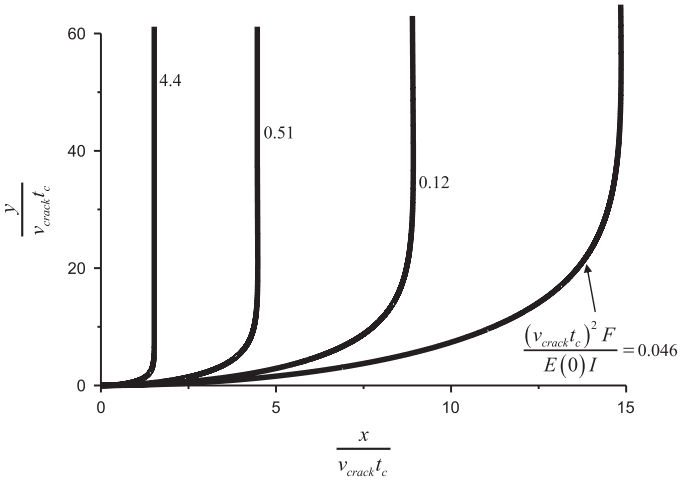

Fig. 3. The profile of the strip for several normalized peel forces for vertical peeling ($\phi = 90^\circ$) and $E(\infty)/E(0) = 0.92$.

Besides the curvature $\kappa = d\theta/ds$, bending moment from Eq. (8), axial force $T = F\cos(\phi-\theta)$, the other variable needed to calculate the energy release rate is membrane strain in the strip

$$\varepsilon_m(s) = \frac{1}{S}\int_0^s J\left(\frac{s-l}{v_{crack}}\right)\frac{dT}{dl}dl = \frac{F}{S}\left\{J(0)\cos[\phi-\theta(s)] + \frac{1}{v_{crack}}\int_0^s \cos[\phi-\theta(l)]J'\left(\frac{s-l}{v_{crack}}\right)dl\right\}, \tag{11}$$

where $S=wh$ is the cross section area, and $J(t)$ is the viscoelastic compliance, which is related to the relaxation modulus by $\int_0^t J(\tau)E(t-\tau)d\tau = t$. For the relaxation modulus $E(t)$ in Eq. (6),

$$J(t) = \frac{1}{E(\infty)} - \left[\frac{1}{E(\infty)} - \frac{1}{E(0)}\right]\exp\left[\frac{-t}{t_c(E(0)/E(\infty))}\right] \tag{12}$$

2.3. Energy release rate

For the strip to delaminate an incremental length dL under the steady-state condition, the work done by the peel force F is (Gent and Hamed, 1975)

$$dW_F = F(1+\varepsilon_{peel}-\cos\phi)dL, \tag{13}$$

where $\varepsilon_{peel} = J(\infty)F/S$ is obtained from Eq. (11) for $s\to\infty$. Similar to Kim and Aravas (1988), the above work equals the sum of energy release $GwdL$ due to interfacial delamination and the change of (elastic and viscoelastic) strain energy dW in the strip,

$$dW_F = GwdL + dW, \tag{14}$$

where G is the energy release rate for interfacial delamination. For steady-state peeling, dW is the product of dL and the change of strain energy stored in a cross section as it goes through the entire strip, i.e., $dW = dL\int_{peeling\ arm} dU$, where $dU = Md\kappa + Td\varepsilon_m$ consists of the bending and membrane energy. Eqs. (13) and (14) then give the energy release rate

$$G = \frac{F}{w}(1+\varepsilon_{peel}-\cos\phi) - \frac{1}{w}\int_{0^-}^{\infty}\left(M\frac{d\kappa}{ds} + T\frac{d\varepsilon_m}{ds}\right)ds. \tag{15}$$

the integration by part of the above equation gives

$$G = \frac{F}{w}(1-\cos\phi) + \frac{1}{w}\int_0^{\infty}\kappa\frac{dM}{ds}ds + \frac{1}{w}\int_0^{\infty}\varepsilon_m\frac{dT}{ds}ds, \tag{16}$$

substitution of Eqs. (8) and (11) into the above equation gives

$$G = \frac{F}{w}\left[1-\cos\phi + g_b + \frac{F}{E(0)A}g_m\right], \tag{17}$$

where g_b and g_m represent contributions from the bending and membrane energies in the strip, respectively, and they are nondimensional functions of normalized peel force $(v_{crack}t_c)^2F/[E(0)I]$, peel angle ϕ, and initial relaxation to long-time asymptote moduli ratio $E(\infty)/E(0)$. Fig. 4 shows g_b and g_m versus the normalized peel force $(v_{crack}t_c)^2F/[E(0)I]$ for peel angle $\phi = 90^\circ$ and $E(\infty)/E(0) = 0.92$; g_b is much less than 1, and g_m is on the order of 1. Therefore, for relatively small peeling strain

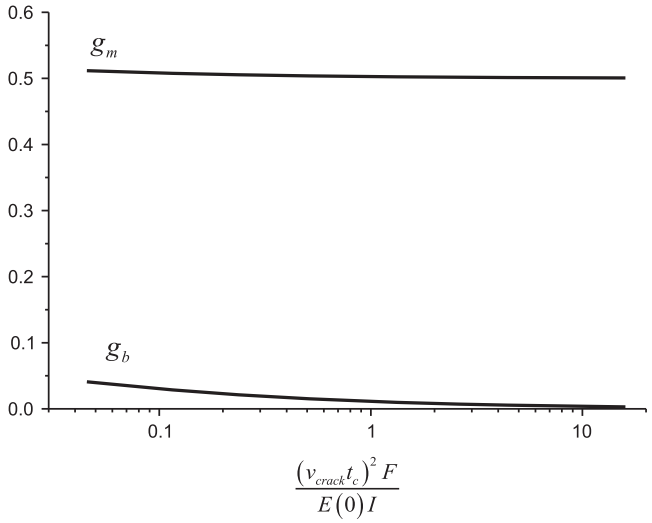

Fig. 4. Parameters g_b and g_m versus the normalized peel force for peel angle $\phi = 90^\circ$ and $E(\infty)/E(0) = 0.92$.

$F/[E(0)S] \ll 1$, the viscoelastic energy release rate has a very simple expression

$$G \approx \frac{F}{w}(1-\cos\phi). \tag{18}$$

3. Interfacial adhesion of a patterned strip

Fig. 5a shows a schematic illustration of a linear viscoelastic strip of width w, with patterned cylindrical pillars at the interface (with a stiff substrate). The cylinders have radius R and height h_{pillar}, and form a rectangular pattern with spacings $a_{\parallel}$ and $a_{\perp}$ parallel and perpendicular to the peel direction, respectively.

3.1. Self-collapse of patterned strips

At relatively large spacing $a_{\parallel}$ and $a_{\perp}$, the patterned strips collapse onto the rigid substrate due to the strip/substrate adhesion. Huang et al. (2005) showed that this self-collapse occurs when the decrease of adhesion energy overwhelms the increase of deformation energy in the strip due to collapse. They established analytically the criterion of self-collapse, which has been validated by experiments (Hsia et al., 2005).

Fig. 5b illustrates the collapsed strip for the pattern in Fig. 5a. The deformation energy in the strip is (Huang et al., 2005)

$$U_{deformation} = 0.617\bar{E}(\infty)h_{pillar}^2 \frac{K(c/(a-2R))}{K[\sqrt{1-(c/(a-2R))^2}]} \frac{((a-2R)/a)^2}{\ln[\sec((\pi/2)(a-2R)/a)]}, \tag{19}$$

where $\bar{E}(\infty) = 4E(\infty)/3$ is the plane-strain modulus for $E(\infty)$ of an incompressible material, K is the complete elliptic integral of first kind, $a = \max(a_{\parallel}, a_{\perp})$ is the larger spacing between $a_{\parallel}$ and $a_{\perp}$, and the collapse length c along a (Fig. 5b) is to be determined. The above equation holds for collapse only along the direction of larger spacing between $a_{\parallel}$ and $a_{\perp}$. Collapse may occur along both directions for large $a_{\parallel}$ and $a_{\perp}$, as studied by Wu et al. (2011). The adhesion energy between the collapsed strip and substrate is

$$U_{adhesion} = -\gamma c, \tag{20}$$

where γ is the work of adhesion, and is around 40 mJ/m^2 to for PDMS/glass (Owen, 1981; Gordon et al., 1998; Aaron et al., 2005; Huang et al., 2005). Minimization of total energy $U_{deformation}+U_{adhesion}$ with respect to c gives the following equation to determine the collapse length c:

$$\frac{d}{dk}\left[\frac{K(k)}{K(\sqrt{1-k^2})}\right]\Bigg|_{k=\frac{c}{a-2R}} = 1.62\frac{\gamma a^2}{\bar{E}(\infty)h_{pillar}^2(a-2R)}\ln\left[\sec\left(\frac{\pi}{2}\frac{a-2R}{a}\right)\right], \tag{21}$$

it suggests that the collapse length c, normalized by $a-2R$, depends on the pillar height, radius and spacing, elastic modulus

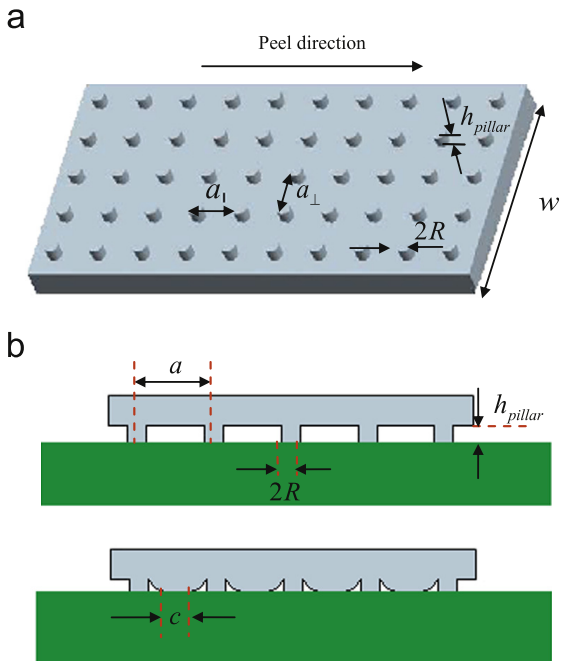

Fig. 5. (a) Schematic illustration of an elastomeric strip with patterned pillars at the interface (with a stiff substrate); (b) illustration of the collapsed strip, where $a = \max(a_{\parallel}, a_{\perp})$.

of the strip, and work of adhesion between the strip and substrate via a single, dimensionless combination λ, i.e.,

$$\frac{c}{a-2R}=\bar{c}(\lambda), \tag{22}$$

where $\bar{c}$ is a nondimensional function of λ, and

$$\lambda=\frac{\gamma a}{\bar{E}(\infty)h_{pillar}^2}\frac{a}{a-2R}\ln\left[\sec\left(\frac{\pi}{2}\frac{a-2R}{a}\right)\right], \tag{23}$$

here $\gamma a/[\bar{E}(\infty)h_{pillar}^2]$ represents the ratio of adhesion energy to deformation energy. Fig. 6 shows the normalized collapse length versus λ. For weak adhesion (or large modulus or height of the pillar or small spacing such that $\lambda<0.238$, Eq. (21) does not have solution for c, which means that self-collapse does not occur. Once λ reaches 0.238, the collapse length immediately jumps from zero to $0.457(a-2R)$, which reflects the nature of instability.

Substitution of c in Eq. (22), or equivalently Fig. 6, into Eq. (19) gives the deformation energy, which takes the form

$$U_{deformation}=\bar{E}(\infty)h_{pillar}^2\frac{((a-2R)/a)^2}{\ln[\sec((\pi/2)(a-2R)/a)]}\bar{U}(\lambda), \tag{24}$$

where $\bar{U}$ is a nondimensional function of a single variable λ. Fig. 7 shows the deformation energy, normalized by $\bar{E}(\infty)h_{pillar}^2[(a-2R)/a]^2/\ln\{\sec[\pi(a-2R)/(2a)]\}$, versus λ. It should be pointed out that Figs. 6 and 7 are the "universal" curves for the collapse length and deformation energy, respectively, since these curves are the same for all materials and geometric parameters.

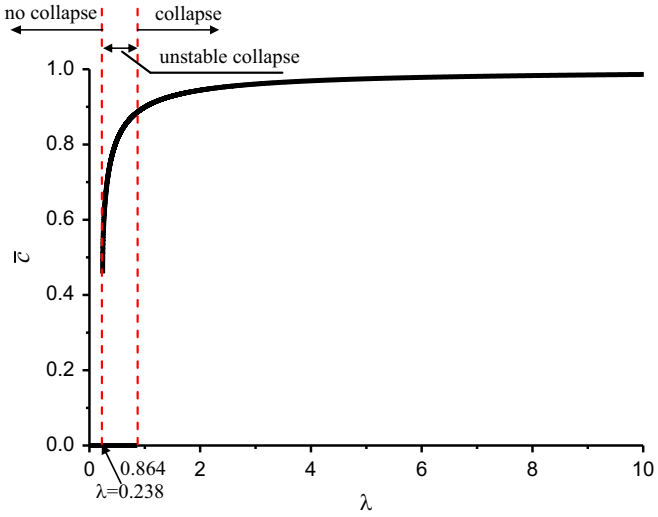

Fig. 6. The normalized collapse length $\bar{c}$ versus λ.

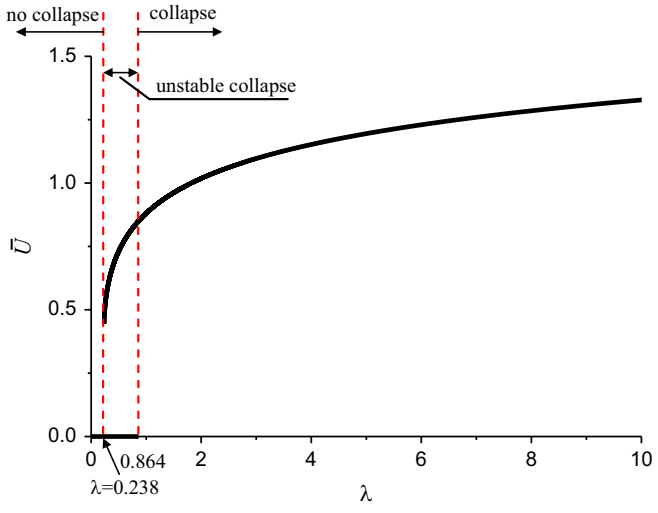

Fig. 7. The normalized deformation energy $\bar{U}$ versus λ.

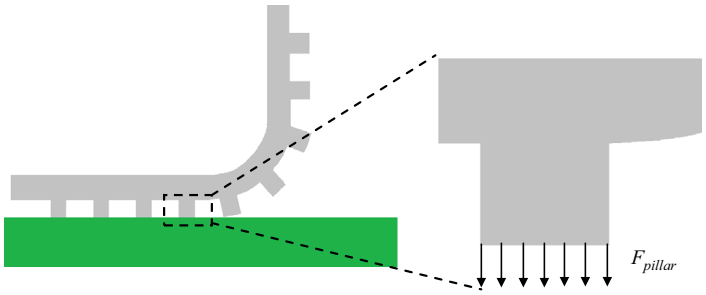

Fig. 8. Schematic illustration of an elastomeric strip with patterned pillars at the interface (with a stiff substrate) in the peel test.

Self-collapse occurs when the total energy $U_{deformation}+U_{adhesion}$ is less than the energy at non-collapsed state (zero). This gives the critical condition for self-collapse as

$$\begin{aligned} &\lambda < 0.864 \Rightarrow \text{no collapse} \\ &\lambda > 0.864 \Rightarrow \text{collapse} \end{aligned} \tag{25}$$

for $0.238 < \lambda < 0.864$, the total energy of collapsed state is higher than zero (of the non-collapsed state). It corresponds to unstable collapse such that it is readily reversible to the non-collapsed state, as indicated by the thick lines coinciding with horizontal axes in Figs. 6 and 7.

3.2. Additional strain energy in the patterned strips

Fig. 8 shows a schematic illustration of the peel test for a linear viscoelastic strip with patterned cylindrical pillars bonded to a stiff substrate. The patterned strips introduces non-uniform deformation in the pillars and strip, which gives additional strain energies stored in pillars and strip beyond that for a flat strip (without patterns) in Section 2.

The net force F_{pillar} on the last pillar before being peeled off from the stiff substrate (Fig. 8) can be obtained from fracture analysis. For an infinitesimal crack to start from the edge, the stress intensity factors are (Tada et al., 2000)

$$K_I = \frac{2}{\pi}\left(0.317\frac{F_{pillar}}{R^{3/2}}\right) \text{and } K_{II} = \frac{2}{\pi}\left(0.103\frac{F_{pillar}}{R^{3/2}}\right), \tag{26}$$

where the factor $2/\pi$ accounts for the cylindrical shape of the pillar. The energy release rate is

$$G = \frac{1}{2}\frac{1}{\bar{E}(0)}(K_I^2 + K_{II}^2) = 0.0225\frac{1}{\bar{E}(0)}\frac{F_{pillar}^2}{R^3}, \tag{27}$$

where $\bar{E}(0)$ is used because the pillar radius R is much less the characteristic length $v_{crack}t_c$ associated with viscoelasticity, and the factor 1/2 accounts for the large elastic mismatch between the strip and substrate (Huang et al., 2005). The above equation then gives

$$F_{pillar} = 6.66\sqrt{\bar{E}(0)GR^3}. \tag{28}$$

The additional strain energy in the last pillar can then be obtained as

$$U_{pillar} = \frac{F_{pillar}^2 h_{pillar}}{2E(0)\cdot\pi R^2} = 9.42GRh_{pillar}, \tag{29}$$

where the pillar is approximately subjected to uniaxial tension. The additional strain energy in the strip can be obtained by modeling the strip as a semi-infinite solid subjected to a uniform pressure of $F_{pillar}/(\pi R^2)$ over a circle of radius R (see Appendix A for details)

$$U_{strip} = 12.0GR^2. \tag{30}$$

3.3. Energy release rate for the patterned strips

The fraction of contact area, i.e., the ratio of strip/substrate contact area to the surface area of the substrate is

$$f = \begin{cases} \pi R^2/(a_\parallel a_\perp) & \text{for} \quad \lambda < 0.864 \\ [\pi R^2 + c\min(a_\parallel, a_\perp)]/(a_\parallel a_\perp) & \text{for} \quad \lambda > 0.864 \end{cases} \tag{31}$$

for the non-collapsed ($\lambda < 0.864$) and collapsed states (($\lambda > 0.864$)), where the collapse length c is given in Eq. (22) and Fig. 6, $\min(a_\parallel, a_\perp)$ is the smaller spacing between $a_\parallel$ and $a_\perp$ and is given by $\min(a_\parallel, a_\perp) = a_\parallel + a_\perp - a$. Let $G_{pattern}$ denote the effective

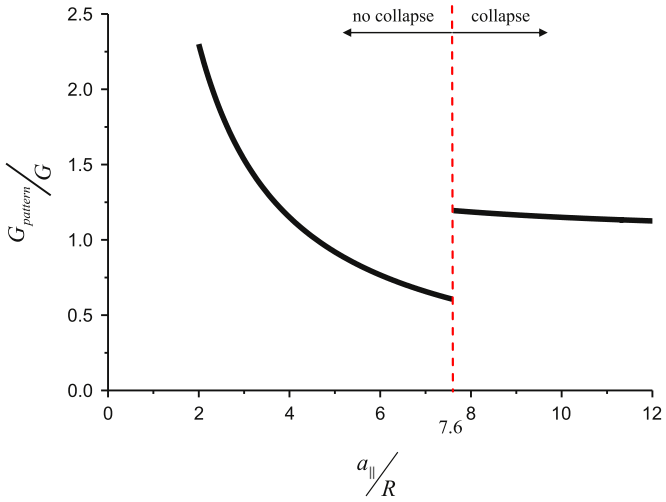

Fig. 9. The normalized effective energy release rate $G_{pattern}/G$ versus the normalized pattern spacing $a_{\parallel}/R$ for $h_{pillar}/R=0.5$, $a_{\perp}/R=4.6$, $\gamma/[\bar{E}(\infty)R]=0.023$, and $G/[\bar{E}(\infty)R]=4.6$ for vanishing crack tip speed.

energy release rate for the patterned strips. For steady-state delamination over length dL of the strip with patterned strips, the effective energy release $G_{pattern}wdL$ consists of the following contributions:

(1) energy release due to delamination over the strip/substrate contact area, $fGwdL$, where f is the contact area fraction in Eq. (31), and G is the energy release rate for a continuous strip given in Eq. (17) or its approximation (i.e. Eq. (18));
(2) release of additional energy in the pillar and strip, $(U_{pillar}+U_{strip})wdL/(a_{\parallel}a_{\perp})$, where $wdL/(a_{\parallel}a_{\perp})$ represents the number of pillars over the area wdL, and U_{pillar} and U_{strip} are given in Eqs. (29) and (30), respectively;
(3) release of deformation energy due to self-collapse, $-U_{deformation}wdL/a$, where $U_{deformation}$ is given in Eq. (24).

These give the effective energy release rate for the patterned strips as

$$G_{pattern}=fG+\frac{U_{pillar}+U_{strip}}{a_{\parallel}a_{\perp}}-\frac{U_{deformation}}{a}, \tag{32}$$

where G is the energy release rate given in Eq. (18) for a flat strip (without patterns). Together with U_{pillar}, U_{strip}, and $U_{deformation}$ in Eqs. (29), (30) and (24), the above equation becomes

$$G_{pattern}=\begin{cases} G\frac{9.42h_{pillar}+15.1R}{a_{\parallel}a_{\perp}}R & \text{for} \quad \lambda<0.864 \\ G\frac{9.42h_{pillar}+15.1R}{a_{\parallel}a_{\perp}}R+\frac{a-2R}{a}\left[G\bar{c}(\lambda)-\gamma\frac{\bar{U}(\lambda)}{\lambda}\right] & \text{for} \quad \lambda>0.864 \end{cases}, \tag{33}$$

where λ is given in Eq. (23), $\bar{c}(\lambda)$ in Eq. (22) and $\bar{U}(\lambda)$ in Eq. (24) are shown in Figs. 6 and 7, respectively. Fig. 9 shows the effective energy release rate $G_{pattern}$ for the patterned strips, normalized by G for a flat strip, versus the normalized pattern spacing $a_{\parallel}/R$ for a set parameters corresponding to the experiments in the next section, $h_{pillar}/R=0.5$, $a_{\perp}/R=4.6$, $\gamma/[\bar{E}(\infty)R]=0.023$, and $G/[\bar{E}(\infty)R]=4.6$ for vanishing crack tip speed. It is observed that, as the pattern spacing $a_{\parallel}$ increases, the effective energy release rate $G_{pattern}$ initially decreases because the fraction of contact area f [in Eq. (31)] decreases. However, once the pattern spacing reaches $a_{\parallel}/R=7.6$, the patterned strips collapse and the contact area increases instantaneously, which leads to the jump of $G_{pattern}$ in Fig. 9. Furthermore, the patterned strips may have smaller energy release rate than that for a flat strip (i.e., $G_{pattern}/G<1$) only if the pattern spacing $a_{\parallel}$ is in the range $(4.3R,7.6R)$ (for the above set of parameters), above which the patterned strips collapse. Below this range the pillars are close such that their strain energy overwhelms the loss of adhesion energy associated with the reduction of contact area of patterned strips (as compared to a flat strip). This has been observed in biologically inspired crack trapping for enhanced adhesion, which shows that the effective adhesion increases when a large contact area is replaced by multiple, small contact areas (e.g., Arzt et al., 2003; Chung and Chaudhury, 2005; Glassmaker et al., 2007). The lower bound of this range is $a_{\parallel}/R=(9.42h_{pillar}+15.1R)/a_{\perp}$ from Eq. (33), while the upper bound of the range is governed by $\lambda=0.864$.

Eq. (33) gives analytically the energy release rate $G_{pattern}$ for a patterned strip once G for a flat strip is measured from experiments. This is very useful to the design of patterned strips since one can adjust the pattern spacing to achieve the desired energy release rate.

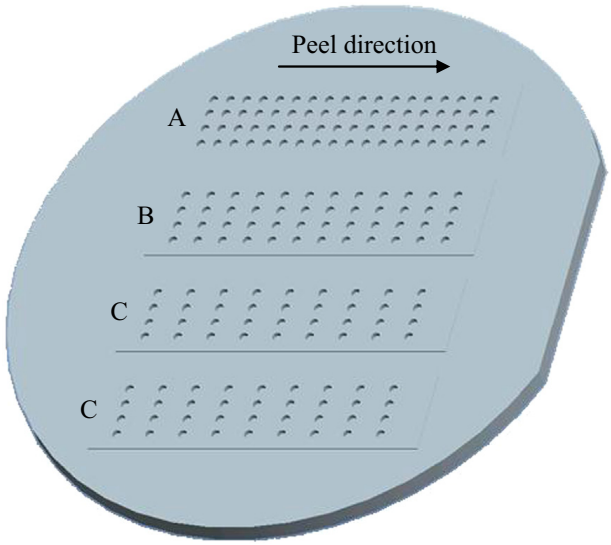

Fig. 10. Schematic illustration of the silicon mold used to fabricate the patterned PDMS. The radius $R=1$ μm, the depth of all the holes is 0.5 μm and the spacing perpendicular to the peel direction $a_\perp = 4.6$ μm. The spacing parallel to the peel direction of these patterns are 4.6, 6.2 and 8.8 μm for patterns A, B and C, respectively.

4. Experiments

4.1. Characterization of materials

The flat PDMS (Sylgard 184 from Dow Corning) was mixed (10:1 and 15:1 ratios) and degassed, poured over a test-grade silicon fixed in a Petri and cured at 30 °C for 96 h. The patterned PDMS was fabricated by pouring the same mixture on a patterned silicon mold, which schematic illustrated in Fig. 10, made by conventional contact mode photolithography process and then also curing at 30 °C for 96 h. Three rectangular patterns of pillars, named A, B and C in Fig. 10, were fabricated. The pillars have radius $R=1$ μm, height $h_{pillar}=0.5$ μm, and the spacing perpendicular to the peel direction $a_\perp = 4.6$ μm. The only difference among these patterns is the spacing parallel to the peel direction, namely 4.6, 6.2 and 8.8 μm for patterns A, B and C, respectively.

Lin et al. (2008) obtained the relaxation modulus of PDMS mixed at 10:1 ratio as

$$E(t) = 1.30 + 0.11e^{-t/0.165}\ (\text{MPa}), \tag{34}$$

where t is in seconds. These give $E(0) = 1.41$ MPa, $E(\infty) = 1.30$ MPa, and $t_c = 0.165$ s, which are also very close to the viscoelastic properties of PDMS mixed at 10:1 ratio reported by others (Choi et al., 2008; Liu et al., 2012). In general, the relaxation moduli increase as the mixing ratio decreases (Armani et al., 1999; Carrillo et al., 2005; Gupta et al., 2007). For PDMS mixed at 15:1 ratio, the elastic modulus is approximately 0.6 times of that for 10:1 ratio (Carrillo et al., 2005), and therefore $E(\infty) = 0.6 \times 1.30 = 0.78$ (MPa) is used for 15:1 ratio in the following.

4.2. Peel test of a flat elastomeric strip (without patterns)

The flat PDMS strips were laminated onto glass slides and left in conformal contact with surface without any extra external force. Inverting the strip/slide (strip side down) and attaching weights to one end of the strip initiated peeling of the PDMS strip from the slide. Pictures from the high-speed camera of each peel event were used to measure the separation speed and the profile of the strip. These pictures were compared to ensure that the interfacial delamination reached steady state. Fig. 11a shows a picture of the steady-state profile of the strip (PDMS mixed at 10:1 ratio, thickness $h=1.18$ mm, and width $w=15.21$ mm). The attached weight is 16.8 g, which gives the peel force $F=0.165$ N (downward, and peel angle $\phi = 90°$). The measured crack tip speed (i.e., speed of interfacial delamination) was $v_{crack}=5.3$ mm/s. These give the normalized force $(v_{crack}t_c)^2F/[E(0)I] = 0.046$, where $E(0)=1.41$ MPa is discussed in Section 4.1. Fig. 11b compares the profile of the strip obtained from Fig. 11a to the analytic solution shown in Fig. 3 for the same normalized force. The analytic solution agrees very well with experiments without any parameter fitting.

In addition to the peel force 0.165 N, the peeling experiments were repeated by the application of a series of constant loads given in Table 1. The measured steady-state crack tip speed (i.e., speed of interfacial delamination) is also given in Table 1, together with the energy release rate obtained from Eq. (18). The energy release rate is shown versus the crack tip speed in Fig. 12, which is well represented by a power law (Gent and Schultz, 1972; Maugis and Barquins, 1978; Tsai and Kim,

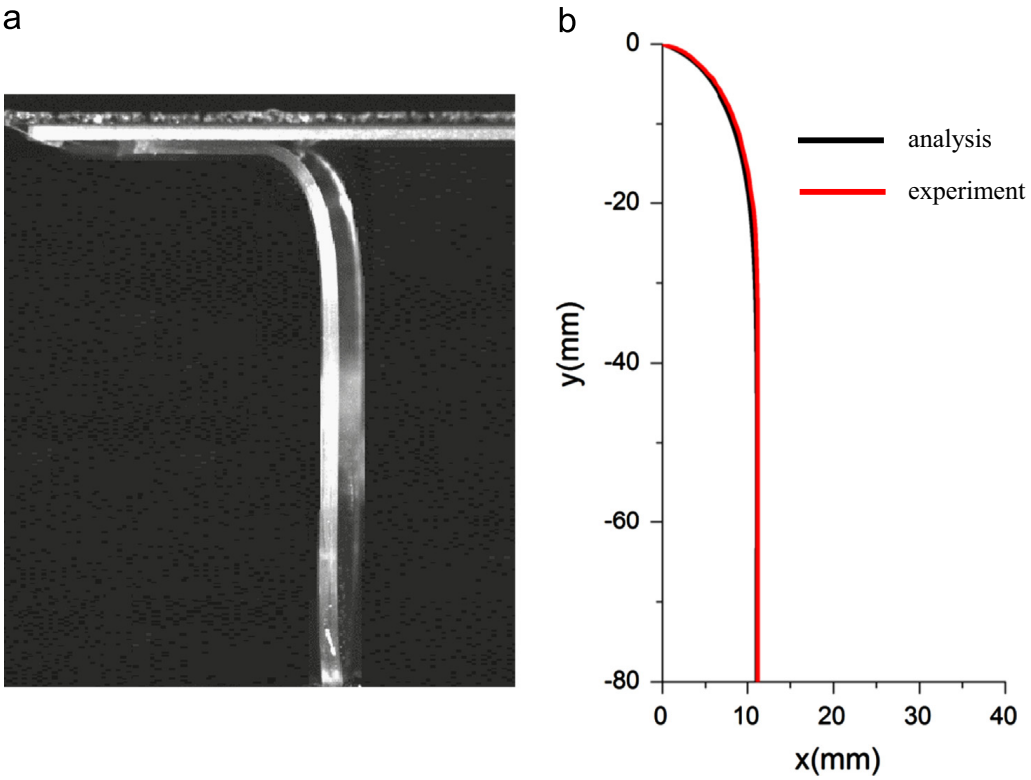

Fig. 11. (a) A picture of the steady-state profile of the strip (PDMS mixed at 10:1 ratio, thickness $h=1.18$ mm, and width $w=15.21$ mm) subject to the peel force $F=0.165$ N; (b) profiles of the strip obtained from the picture in (a) and the analytic solution shown in Fig. 3 for the same peel force.

Table 1
Peel test for PDMS mixed at 10:1 ratio.

Peel force (N)	0.165	0.201	0.233	0.253	0.270	0.294	0.317	0.387
Energy release rate (J/m^2)	11	14	15	16	18	19	21	25
Crack tip speed (mm/s)	5.3	7.5	11	15	23	31	38	65

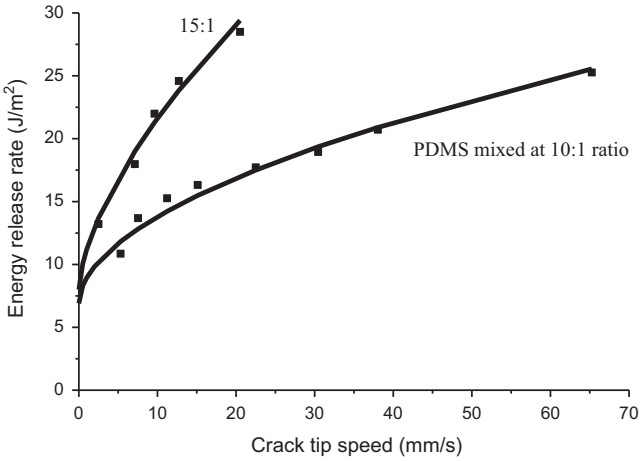

Fig. 12. The energy release rate versus the crack tip speed for PDMS mixed at 10:1 and 15:1 ratios, and the power-law relation.

1993; Barquins and Ciccotti, 1997; Barthel and Roux, 2000; Feng et al., 2007)

$$G(v_{crack}) = G_0\left[1+\left(\frac{v_{crack}}{v_0}\right)^n\right], \tag{35}$$

where G_0 is the energy release rate at a vanishing crack tip speed, and v_0 is a reference speed. For PDMS mixed at 10:1 ratio, $G_0=6.9$ J/m^2, $v_0=10$ mm/s, and exponent $n=0.53$. The experimental results for PDMS mixed at 15:1 ratio are also shown in

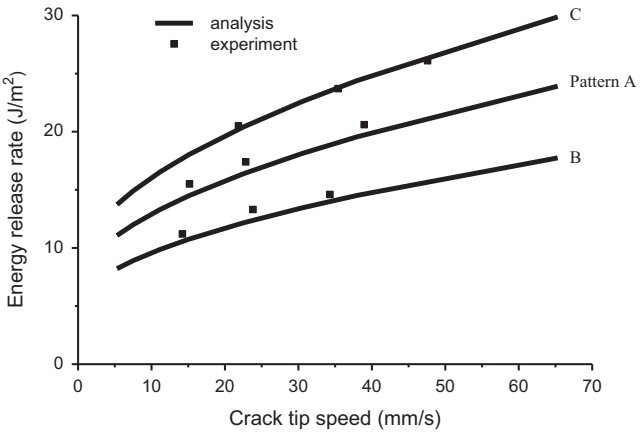

Fig. 13. The energy release rate versus the crack tip speed for the patterned PDMS strip mixed at 10:1 ratio. Three patterns A, B and C correspond to those illustrated in Fig. 10, which have the radius $R=1$ μm, the depth 0.5 μm and the spacing perpendicular to the peel direction $a_\perp = 4.6$ μm. The spacing parallel to the peel direction of these patterns are 4.6, 6.2 and 8.8 μm for patterns A, B and C, respectively.

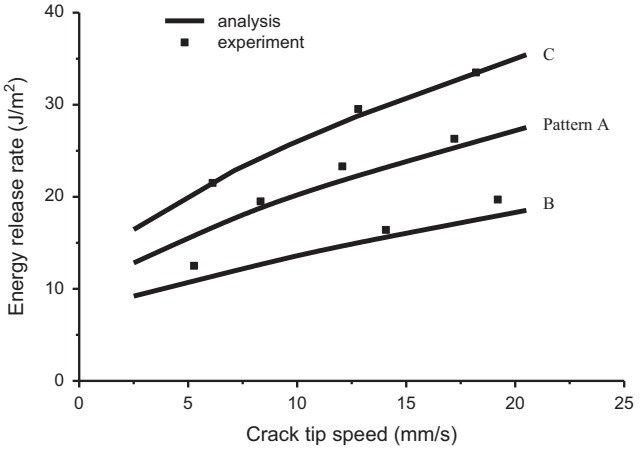

Fig. 14. The energy release rate versus the crack tip speed for the patterned PDMS strip mixed at 15:1 ratio. Three patterns A, B and C correspond to those illustrated in Fig. 10, which have the radius $R=1$ μm, the depth 0.5 μm and the spacing perpendicular to the peel direction $a_\perp = 4.6$ μm. The spacing parallel to the peel direction of these patterns are 4.6, 6.2 and 8.8 μm for patterns A, B and C, respectively.

Fig. 12, which give $G_0=8.0$ J/m^2, $v_0=4.3$ mm/s, and $n=0.63$. The energy release rate increases with the crack tip speed [Fig. 12; Eq. (35)] because, as the rate increases, more energy is dissipated through viscous effect.

4.3. *Peel test of an elastomeric strip with patterned strips*

The uniform part of the patterned PDMS strips had the same thickness as the flat strips as in Section 4.2 but smaller width around 10 mm. The pillar size and spacing were described in Section 4.1. The patterned PDMS strips were also laminated onto glass slides, left in conformal contact with surface without any extra external force, and initiated peeling of the PDMS strip from the slide by attaching weights to one end of the strip.

For each pattern (A, B or C), three weights were used, which gave the peel force 0.114, 0.135 and 0.144 N for pattern A; 0.156, 0.172 and 0.201 N for pattern B; and 0.201, 0.233 and 0.259 N for pattern C. The ratio of each force to the width of the corresponding strip then gave the experimentally obtained energy release rate according to Eq. (18). The steady-state crack tip speed was measured by the same method as that in Section 4.2 for a flat strip. The steady state of measured profile is reached at a scale ~10 mm (e.g., Fig. 12), which is much larger than the pattern spacing (~1 μm).

For PDMS mixed at 10:1 ratio, Fig. 13 shows the experimentally measured energy release rate versus the crack tip speed for patterns A, B and C, where the energy release rate was obtained from the peel force via Eq. (18). Fig. 13 also shows the analytically predicted energy release rate from Eq. (33), which only involves the pillar size and spacing, the power-law relation$G(v_{crack})$ in Eq. (35) for the flat strip (without patterns), and work of adhesion $\gamma=41$ mJ/m^2 , which agrees with the literature value (Owen, 1981; Gordon et al., 1998). The analytic model agrees well with experiments for all three patterns and the large range of crack tip speed, and therefore can be used to design the patterned strips to achieve the desired energy release rate. The energy release rate for pattern A, which has the smallest pattern spacing, is very close to G for the flat strip in Fig. 12. Pattern B has a larger spacing than pattern A; its energy release rate is the smallest among all three patterns

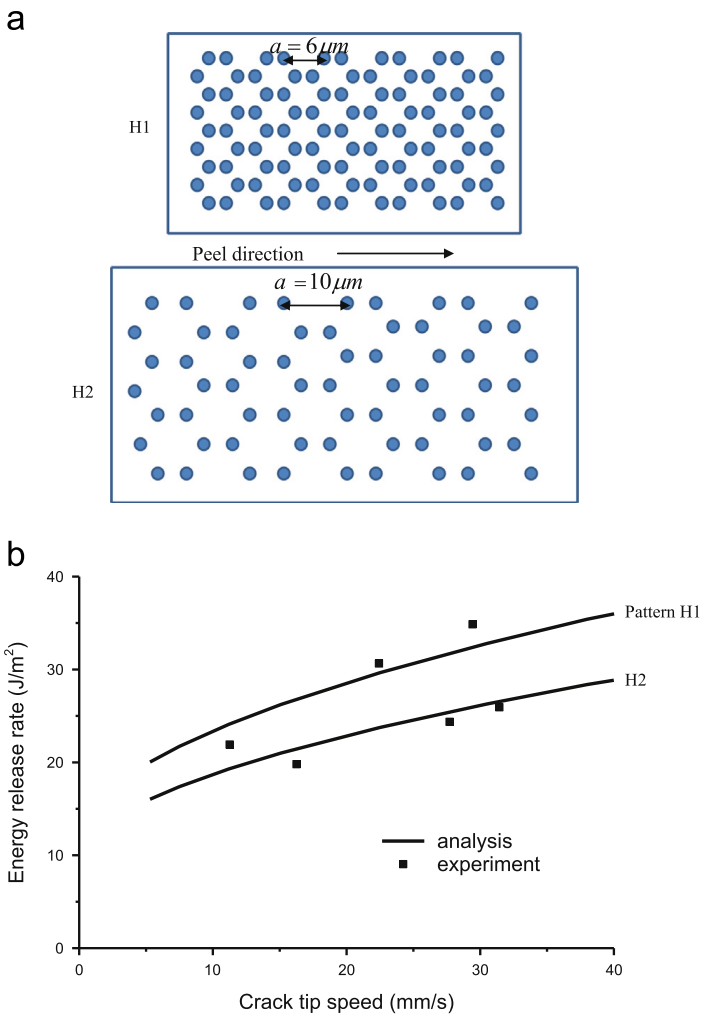

Fig. 15. (a) Schematic illustration of the hexagonal patterns H1 ($a = 6\ \mu m$) and H2 ($a = 10\ \mu m$); (b) the energy release rate versus the crack tip speed for the PDMS strip with hexagonal patterns mixed at 10:1 ratio.

(Fig. 13), and is much lower than G for the flat strip (Fig. 12). Pattern C has the largest spacing, but its energy release rate is the largest among the three (Fig. 13), and is much higher than G for the flat strip (Fig. 12). This non-monotonic behavior agrees well with the analytic model since Eq. (33) predicts no collapse for patterns A and B ($\lambda < 0.864$), but collapse for pattern C ($\lambda > 0.864$).

This non-monotonic dependence of energy release rate on pattern spacing is also observed in Fig. 14 for PDMS mixed at 15:1 ratio for the same three patterns. Once again the energy release rate for pattern A is between those for patterns B and C. For all three patterns, the analytic model in Eq. (33) agrees well with experiments for the power-law relation$G(v_{crack})$ in Eq. (35) for PDMS mixed at 15:1 and slight larger work of adhesion γ=41 mJ/m^2 because the material is more viscous than PDMS mixed at 10:1 ratio.

5. Concluding remarks and discussions

The analytic solution for peel test of a viscoelastic strip on substrate is obtained, and is validated by the profile of PDMS peel arm measured in experiments. It establishes a simple way to determine the energy release rate as a function of the crack tip speed for delamination of strip/substrate interface. The analytic solution for patterned strips is also obtained and validated by experiments. It provides a useful way to design patterned strips to achieve the desired interfacial properties, either stronger or weaker than those for a flat strip (without patterns). As an example, the pattern spacing is shown, both analytically and experimentally, to control the energy release rate. As the pattern spacing increases, the energy release rate for patterned strips initially decreases and becomes smaller than that for a flat strip, but it has a sudden jump to be significantly larger once the pattern spacing reaches a critical value, at which the patterned strips self-collapse onto the substrate and thereby significantly increase the contact area.

The effective energy release rate in Eq. (33) is also applicable to other patterns by replacing $a_{\parallel}a_{\perp}$ with the average area A per pillar while keeping a as the maximum spacing among neighbor pillars, as illustrated in Fig. 15a for two hexagon

patterns H1 and H2 for $a=6\,\mu m$ and $10\,\mu m$, respectively. The effective energy release rate becomes

$$G_{pattern}=\begin{cases} G\frac{9.42h_{pillar}+15.1R}{A}R & \text{for} \quad \lambda<0.864 \\ G\frac{9.42h_{pillar}+15.1R}{A}R+\frac{a-2R}{a}\left[G\bar{c}(\lambda)-\gamma\frac{\bar{U}(\lambda)}{\lambda}\right] & \text{for} \quad \lambda>0.864 \end{cases}, \tag{36}$$

where G is the energy release rate given in Eq. (18) for a flat strip (without patterns), λ is given in Eq. (23), $\bar{c}(\lambda)$ in Eq. (22) and $\bar{U}(\lambda)$ in Eq. (24) are shown in Figs. 6 and 7, respectively. Peel tests were conducted for 10:1 PDMS strips with two hexagonal patterns of pillars, H1 and H2 illustrated in Fig. 15a. The pillars have radius $R=1\,\mu m$, height $h_{pillar}=0.5\,\mu m$, and maximum spacing $a=6\,\mu m$ or $10\,\mu m$. Fig. 15b shows the experimentally measured energy release rate versus the crack tip speed for patterns H1 and H2. It also shows the analytically predicted energy release rate from Eq. (36) based on the same power-law relation$G(v_{crack})$ in Eq. (35), and the same work of adhesion $\gamma=41\ mJ/m^2$. The analytic model agrees well with experiments for two hexagonal patterns without any parameter fitting.[1] It should be pointed out that Eq. (36), as well as the analytic model in Section 3, are for patterned cylindrical pillars, and are not applicable to other shapes such as parallel lines (Kim et al., 2009).

Acknowledgments

X.F. acknowledges the support from National Natural Science Foundation of China (Grant nos. 90816007, 91116006, and 10902059), Tsinghua University Initiative Scientific Research Program (No. 2011Z02173) and Foundation for the Author of National Excellent Doctoral Dissertation of China (FANEDD) (No. 2007B30). Y.H. and J.A.R. acknowledge the support from NSF (Grant nos. CMMI-0749028 and ECCS-0824129) and INSPIRE.

Appendix A. Tangential velocity of the strip

The length L of delaminated interface in the original, outstretched state is related to the current length s_L of the peeling arm by

$$L=\int_0^{s_L}\frac{ds}{1+\varepsilon_m(s,t)}, \tag{A.1}$$

where $\varepsilon_m(s,t)$ is the membrane strain and it depends on time t. The speed of interfacial delamination is

$$v_{crack}=\frac{dL}{dt}=\frac{ds_L}{dt}\frac{1}{1+\varepsilon^c(s_L,t)}-\int_0^{s_L}\frac{(\partial\varepsilon^c(s,t))/\partial t}{[1+\varepsilon^c(s,t)]^2}ds, \tag{A.2}$$

for steady-state delamination of the interface, ε_m not depend on t explicitly such that the above equation becomes

$$v_{crack}=\frac{dL}{dt}=\frac{ds_L}{dt}\frac{1}{1+\varepsilon_m(s_L)}=\frac{v_{peel}}{1+\varepsilon_{peel}}, \tag{A.3}$$

where ε_{peel} is the axial strain at the end of the peeling arm, and v_{peel} is the peeling speed. Elimination of v_{carck} gives the tangential velocity in Eq. (7).

A.1. Strain energy in the strip

The additional strain energy in the strip can be obtained by modeling the strip as a semi-infinite solid subjected to a uniform pressure of $F_{pillar}/(\pi R^2)$ over a circle of radius R. The normal displacement at the pillar/strip interface is given by (Johnson, 1987)

$$u_n(\rho)=\frac{4R}{\pi\bar{E}(0)}\frac{F_{pillar}}{\pi R^2}E\left(\frac{\rho}{a}\right), \tag{A.4}$$

where E is the complete elliptic integration of second kind (note, here E is not to be confused with the relaxation modulus). Integration of the above displacement, together with the pressure $F_{pillar}/(\pi R^2)$ and Eq. (28), gives the strain energy in the strip in Eq. (30).

References

Aaron, M.F., Wenhua, Z., Alfred, J.C., Christopher, M.S., 2005. A multilens measurement platform for high-throughput adhesion measurements. Meas. Sci. Technol. 16, 81.

[1] The PDMS strips with rectangular and hexagonal patterns were fabricated at different time, and showed slightly different material properties. We have verified that the agreement between the analysis and experiments in Fig. 15b becomes even better if the differences in material properties are accounted for.

Armani, D., Liu, C., Aluru, N., 1999. Re-configurable fluid circuits by PDMS elastomer micromachining. In: Proceedings of the Twelfth IEEE International Conference on Micro Electro Mechanical Systems, 1999. MEMS '99, pp. 222–227.
Arzt, E., Gorb, S., Spolenak, R., 2003. From micro to nano contacts in biological attachment devices. Proc. Natl. Acad. Sci. 100, 10603–10606.
Barquins, M., Ciccotti, M., 1997. On the kinetics of peeling of an adhesive tape under a constant imposed load. Int. J. Adhes. Adhes. 17, 65–68.
Barthel, E., Roux, S., 2000. Velocity-dependent adherence: an analytical approach for the JKR and DMT models. Langmuir 16, 8134–8138.
Bikerman, J.J., 1957. Theory of peeling through a hookean solid. J. Appl. Phys. 28, 1484–1485.
Brown, H.R., 1991. The adhesion between polymers. Annu. Rev. Mater. Sci. 21, 463–489.
Carlson, A., Bowen, A.M., Huang, Y.G., Nuzzo, R.G., Rogers, J.A., 2012a. Transfer printing techniques for materials assembly and micro/nanodevice fabrication. Adv. Mater. 24, 5284–5318.
Carlson, A., Kim-Lee, H.-J., Wu, J., Elvikis, P., Cheng, H., Kovalsky, A., Elgan, S., Yu, Q., Ferreira, P.M., Huang, Y., Turner, K.T., Rogers, J.A., 2011. Shear-enhanced adhesiveless transfer printing for use in deterministic materials assembly. Appl. Phys. Lett. 98, 264104.
Carlson, A., Wang, S., Elvikis, P., Ferreira, P.M., Huang, Y., Rogers, J.A., 2012b. Active, programmable elastomeric surfaces with tunable adhesion for deterministic assembly by transfer printing. Adv. Funct. Mater. 22, 4476–4484.
Carrillo, F., Gupta, S., Balooch, M., Marshall, S.J., Marshall, G.W., Pruitt, L., Puttlitz, C.M., 2005. Nanoindentation of polydimethylsiloxane elastomers: effect of crosslinking, work of adhesion, and fluid environment on elastic modulus. J. Mater. Res. 20, 2820–2830.
Cheng, H., Wu, J., Yu, Q., Kim-Lee, H.-J., Carlson, A., Turner, K.T., Hwang, K.-C., Huang, Y., Rogers, J.A., 2012. An analytical model for shear-enhanced adhesiveless transfer printing. Mech. Res. Commun. 43, 46–49.
Choi, S.T., Jeong, S.J., Earmme, Y.Y., 2008. Modified-creep experiment of an elastomer film on a rigid substrate using nanoindentation with a flat-ended cylindrical tip. Scri. Mater. 58, 199–202.
Christensen, R.M., 2003. Theory of Viscoelasticity, second edition, Dover Publications, Inc.
Chung, J.Y., Chaudhury, M.K., 2005. Roles of discontinuities in bio-inspired adhesive pads. J. R. Soc. Interface 2, 55–61.
Crosby, A.J., Hageman, M., Duncan, A., 2005. Controlling polymer adhesion with “pancakes”. Langmuir 21, 11738–11743.
Feng, X., Meitl, M.A., Bowen, A.M., Huang, Y., Nuzzo, R.G., Rogers, J.A., 2007. Competing fracture in kinetically controlled transfer printing. Langmuir 23, 12555–12560.
Gao, H., Yao, H., 2004. Shape insensitive optimal adhesion of nanoscale fibrillar structures. Proc. Natl. Acad. Sci. USA 101, 7851–7856.
Gardon, J.L., 1963. Peel adhesion. II. A theoretical analysis. J. Appl. Polym. Sci. 7, 643–665.
Geim, A.K., Dubonos, S.V., Grigorieva, I.V., Novoselov, K.S., Zhukov, A.A., Shapoval, S.Y., 2003. Microfabricated adhesive mimicking gecko foot-hair. Nat. Mater. 2, 461–463.
Gent, A.N., 1996. Adhesion and strength of viscoelastic solids. Is there a relationship between adhesion and bulk properties? Langmuir 12, 4492–4496.
Gent, A.N., Hamed, G.R., 1975. Peel mechanics. J. Adhes. 7, 91–95.
Gent, A.N., Schultz, J., 1972. Effect of wetting liquids on strength of adhension of viscoelastic materials. J Adhes. 3, 281.
Glassmaker, N.J., Jagota, A., Hui, C.Y., Noderer, W.L., Chaudhury, M.K., 2007. Biologically inspired crack trapping for enhanced adhesion. Proc. Natl. Acad. Sci. USA 104, 10786–10791.
Gordon, G.V., Perz, S.V., Tabler, R.L., Stasser, J.L., Owen, M.J., Tonge, J.S., 1998. .
Gupta, S., Carrillo, F., Li, C., Pruitt, L., Puttlitz, C., 2007. Adhesive forces significantly affect elastic modulus determination of soft polymeric materials in nanoindentation. Mater. Lett. 61, 448–451.
Hsia, K.J., Huang, Y., Menard, E., Park, J.U., Zhou, W., Rogers, J., Fulton, J.M., 2005. Collapse of stamps for soft lithography due to interfacial adhesion. Appl. Phys. Lett. 86, 154106.
Huang, Y.G.Y., Zhou, W.X., Hsia, K.J., Menard, E., Park, J.U., Rogers, J.A., Alleyne, A.G., 2005. Stamp collapse in soft lithography. Langmuir 21, 8058–8068.
Hui, C.Y., Glassmaker, N.J., Jagota, A., 2005. How compliance compensates for surface roughness in fibrillar adhesion. J. Adhes. 81, 699–721.
Johnson, K.L., 1987. Contact Mechanics. Cambridge University Press, Cambridge.
Johnson, K.L., Kendall, K., Roberts, A.D., 1971. Suface energy and contact of elastic solids. Proc. R. Soci. London Ser. A 324, 301.
Jouwersma, C., 1960. On the theroy of peeling. J. Polym. Sci. 45, 253–255.
Jung, I., Shin, G., Malyarchuk, V., Ha, J.S., Rogers, J.A., 2010. Paraboloid electronic eye cameras using deformable arrays of photodetectors in hexagonal mesh layouts. Appl. Phys. Lett. 96, 021110–021113.
Kaeble, D.H., 1959. Theory and analysis of peel adhesion: mechanisms and mechanics. Trans. Soc. Rheol. 3, 161.
Kaeble, D.H., 1960. Theory and analysis of peel adhesion: bond stresses and distributions. Trans. Soc. Rheol. 4, 45.
Kendall, K., 1973. Peel adhesion of solid films—surface and bulk effects. J. Adhes. 5, 179–202.
Kendall, K., 1975. Thin-film peeling—elastic term. J. Phys. D Appl. Phys. 8, 1449–1452.
Kim, D.-H., Lu, N., Ghaffari, R., Kim, Y.-S., Lee, S.P., Xu, L., Wu, J., Kim, R.-H., Song, J., Liu, Z., Viventi, J., de Graff, B., Elolampi, B., Mansour, M., Slepian, M.J., Hwang, S., Moss, J.D., Won, S.-M., Huang, Y., Litt, B., Rogers, J.A., 2011a. Materials for multifunctional balloon catheters with capabilities in cardiac electrophysiological mapping and ablation therapy. Nat. Mater. 10, 316–323.
Kim, D.-H., Lu, N., Ma, R., Kim, Y.S., Kim, R.H., Wang, S., Wu, J., Won, S.M., Tao, H., Islam, A., Yu, K.J., Kim, T.I., Chowdhury, R., Ying, M., Xu, L., Li, M., Chung, H.J., Keum, J.A., McCormick, M., Liu, P., Zhang, Y.W., Omenetto, F.G., Huang, Y., Coleman, T., Rogers, J.A., 2011b. Epidermal Electron. Sci. (New York, NY) 333, 838–843.
Kim, D.-H., Viventi, J., Amsden, J.J., Xiao, J., Vigeland, L., Kim, Y.-S., Blanco, J.A., Panilaitis, B., Frechette, E.S., Contreras, D., Kaplan, D.L., Omenetto, F.G., Huang, Y., Hwang, K.-C., Zakin, M.R., Litt, B., Rogers, J.A., 2010a. Dissolvable films of silk fibroin for ultrathin conformal bio-integrated electronics. Nat. Mater. 9, 511–517.
Kim, J., Kim, K.S., Kim, Y.H., 1989. Mechanical effects in peel adhesion test. J. Adhes. Sci. Technol. 3, 175–187.
Kim, K.S., Aravas, N., 1988. Elastoplastic analysis of the peel test. Int. J. Solids Struct. 24, 417–435.
Kim, R.-H., Kim, D.-H., Xiao, J., Kim, B.H., Park, S.-I., Panilaitis, B., Ghaffari, R., Yao, J., Li, M., Liu, Z., Malyarchuk, V., Kim, D.G., Le, A.-P., Nuzzo, R.G., Kaplan, D.L., Omenetto, F.G., Huang, Y., Kang, Z., Rogers, J.A., 2010b. Waterproof AlInGaP optoelectronics on stretchable substrates with applications in biomedicine and robotics. Nat. Mater. 9, 929–937.
Kim, S., Carlson, A., Huanyu, C., Seungwoo, L., Jung-Ki, P., Yonggang, H., Rogers, J.A., 2012. Enhanced adhesion with pedestal-shaped elastomeric stamps for transfer printing. Appl. Phys. Lett. 100, 171909.
Kim, S., Wu, J., Carlson, A., Jin, S.H., Kovalsky, A., Glass, P., Liu, Z., Ahmed, N., Elgan, S.L., Chen, W., Ferreira, P.M., Sitti, M., Huang, Y., Rogers, J.A., 2010c. Microstructured elastomeric surfaces with reversible adhesion and examples of their use in deterministic assembly by transfer printing. Proc. Natl. Acad. Sci. USA 107, 17095–17100.
Kim, T.-H., Carlson, A., Ahn, J.-H., Won, S.M., Wang, S., Huang, Y., Rogers, J.A., 2009. Kinetically controlled, adhesiveless transfer printing using microstructured stamps. Appl Phys Lett. 94, 113502.
Ko, H.C., Stoykovich, M.P., Song, J., Malyarchuk, V., Choi, W.M., Yu, C.-J., Geddes Iii, J.B., Xiao, J., Wang, S., Huang, Y., Rogers, J.A., 2008. A hemispherical electronic eye camera based on compressible silicon optoelectronics. Nature 454, 748–753.
Lamblet, M., Verneuil, E., Vilmin, T., Buguin, A., Silberzan, P., Leger, L., 2007. Adhesion enhancement through micropatterning at polydimethylsiloxane-acrylic adhesive interfaces. Langmuir 23, 6966–6974.
Li, R., Li, Y., Lü, C., Song, J., Saeidpourazar, R., Fang, B., Zhong, Y., Ferreira, P., Rogers, J., Huang, Y., 2012a. Axisymmetric thermo-mechanical analysis of laser-driven non-contact transfer printing. Int. J. Fract. 176, 189–194.
Li, R., Li, Y., Lu, C., Song, J., Saeidpouraza, R., Fang, B., Zhong, Y., Ferreira, P.M., Rogers, J.A., Huang, Y., 2012b. Thermo-mechanical modeling of laser-driven non-contact transfer printing: two-dimensional analysis. Soft Matter 8, 7122–7127.
Lin, I.K., Liao, Y.-M., Liu, Y., Ou, K.-S., Chen, K.-S., Zhang, X., 2008. Viscoelastic mechanical behavior of soft microcantilever-based force sensors. Appl. Phys. Lett. 93, 251903–251907.

Liu, X., Shi, J., Zong, Z., Wan, K.-T., Sun, Y., 2012. Elastic and viscoelastic characterization of mouse oocytes using micropipette indentation. Ann. Biomed Eng. 40, 2122–2130.
Loukis, M.J., Aravas, N., 1991. The effects of viscoelasticity in the peeling of polymeric films. J. Adhes. 35, 7–22.
Maugis, D., Barquins, M., 1978. Fracture mechanics and adherence of viscoelastic bodies. J. Phys. D Appl. Phys. 11, 1989.
Meitl, M.A., Zhu, Z.T., Kumar, V., Lee, K.J., Feng, X., Huang, Y.Y., Adesida, I., Nuzzo, R.G., Rogers, J.A., 2006. Transfer printing by kinetic control of adhesion to an elastomeric stamp. Nat. Mater. 5, 33–38.
Nicholson, D.W., 1977. Peel mechanics with large bending. Int. J. Fract. 13, 279–287.
Owen, M.J., 1981. Surface tension of silicone release paper coatings. J. Coat. Technol. 679, 4.
Persson, B.N.J., Gorb, S., 2003. The effect of surface roughness on the adhesion of elastic plates with application to biological systems. J. Chem. Phys. 119, 11437–11444.
Poulard, C., Restagno, F., Weil, R., Leger, L., 2011. Mechanical tuning of adhesion through micro-patterning of elastic surfaces. Soft Matter 7, 2543–2551.
Saeidpourazar, R., Li, R., Li, Y., Sangid, M.D., Lu, C., Huang, Y., Rogers, J.A., Ferreira, P.M., 2012. Laser-driven micro transfer placement of prefabricated microstructures. J. Microelectromech. Syst. 21, 1049–1058.
Someya, T., Sekitani, T., Iba, S., Kato, Y., Kawaguchi, H., Sakurai, T., 2004. A large-area, flexible pressure sensor matrix with organic field-effect transistors for artificial skin applications. Proce. Natl. Acad. Sci. USA 101, 9966–9970.
Spies, G.J., 1953. The peeling test on redux-bonded joints. J. Aircr. Eng. 25, 64.
Tada, H., Paris, P.C., Irwin, G.R., 2000. The Stress Analysis of Cracks Handbook. Asme Press, New York.
Tsai, K.H., Kim, K.S., 1993. Stick-slip in the thun-film peel test. 1. The 90-degrees peel test. Int. J. Solids Struct. 30, 1789–1806.
Viventi, J., Kim, D.-H., Moss, J.D., Kim, Y.-S., Blanco, J.A., Annetta, N., Hicks, A., Xiao, J., Huang, Y., Callans, D.J., Rogers, J.A., Litt, B., 2010. A conformal, bio-interfaced class of silicon electronics for mapping cardiac electrophysiology. Sci. Transl. Med. 2 (16), 24ra22.
Viventi, J., Kim, D.-H., Vigeland, L., Frechette, E.S., Blanco, J.A., Kim, Y.-S., Avrin, A.E., Tiruvadi, V.R., Hwang, S.-W., Vanleer, A.C., Wulsin, D.F., Davis, K., Gelber, C.E., Palmer, L., Van der Spiegel, J., Wu, J., Xiao, J., Huang, Y., Contreras, D., Rogers, J.A., Litt, B., 2011. Flexible, foldable, actively multiplexed, high-density electrode array for mapping brain activity in vivo. Nat. Neurosci. 14, 1599-U1138.
Wu, J., Kim, S., Chen, W., Carlson, A., Hwang, K.-C., Huang, Y., Rogers, J.A., 2011. Mechanics of reversible adhesion. Soft Matter 7, 8657–8662.
Yang, S.Y., Carlson, A., Cheng, H., Yu, Q., Ahmed, N., Wu, J., Kim, S., Sitti, M., Ferreira, P.M., Huang, Y., Rogers, J.A., 2012. Elastomer surfaces with directionally dependent adhesion strength and their use in transfer printing with continuous roll-to-roll applications. Adv. Mater. 24, 2117–2122.
Yao, H., Gao, H., 2006. Mechanics of robust and releasable adhesion in biology: bottom-up designed hierarchical structures of gecko. J. Mech. Phys. Solids 54, 1120–1146.
Yurenka, S., 1962. Peel testing of adhesive bonded metal. J. Appl. Polym. Sci. 6, 136–144.